Optical-phonon behavior in $Ga_{1-x}In_xAs$: The role of microscopic strains and ionic plasmon coupling

J. Groenen, R. Carles, and G. Landa
Laboratoire de Physique des Solides, Université P. Sabatier, 118 route de Narbonne, 31062 Toulouse Cedex 4, France

C. Guerret-Piécourt and C. Fontaine
Laboratoire d'Architecture et d'Analyse des Systèmes, Avenue E. Belin, 31077 Toulouse Cedex 4, France

M. Gendry
Ecole Centrale de Lyon, Laboratoire d'électronique, LEAME, Boîte Postale 163, 69131 Ecully Cedex, France
(Received 22 May 1998)

We present an experimental and theoretical investigation of long-wavelength optical-phonon behavior in $Ga_{1-x}In_xAs$ alloys. We propose a model which accounts quantitatively for both phonon frequencies and Raman intensities. The transverse-optical-phonon behavior is shown to be determined by mass disorder and microscopic strains. It is shown that Raman scattering provides a means of measuring local bond distortions in mixed crystals. Coupling by the macroscopic ionic polarization is shown to determine the longitudinal optical-phonon behavior. The model accounts for the so-called anomalies of the Raman intensities and oscillator strengths observed in $Ga_{1-x}In_xAs$. Our analysis is supported by a thorough Raman-scattering study. The frequencies, Raman intensities and symmetries of both the transverse- and longitudinal-optical modes have been determined accurately over the whole compositional range, by using different crystal orientations ([001], [110], and [111]). [S0163-1829(98)07540-7]

I. INTRODUCTION

The behavior of long-wavelength optical phonons in $A_{1-x}B_xC$ alloys has been the subject of a great deal of experimental and theoretical work. This behavior is usually categorized according to two classes, two-mode or persistent type and one-mode or amalgamation type. In the two mode type, two bands of frequencies (close to those of the AC and BC binaries) persist in the mixed crystal. The strength of each band in the Raman or infrared reflectivity (IR) spectra grows from zero to the maximum as the concentration of the corresponding constituent is increased. In the one-mode type, the band varies continuously from the characteristic AC frequencies to the BC ones, with the strength of the band remaining almost constant. Most of the III-V alloys display two-mode behavior ($Ga_{1-x}Al_xAs$,[1–3] $Ga_{1-x}Al_xSb$,[4,5] $InAs_xP_{1-x}$,[6,7] $In_xAl_{1-x}As$,[8,9] etc. Even $Ga_{1-x}In_xP$, which was first thought to belong to the one-mode type, was finally shown to display two-mode behavior.[10] $Ga_{1-x}Al_xN$ was recently shown to have one-mode behavior.[11]

The optical-phonon behavior in $Ga_{1-x}In_xAs$ was originally referred to as the mixed mode or one-two mode by Brodsky and Luckovsky.[12] $Ga_{1-x}In_xAs$ Raman and IR spectra indeed display a rather odd behavior. InAs-like features were hardly detected in the spectra at low In contents, and their intensities were found still to be low at higher In contents. Although it has been investigated in many works,[12–19] a full description of this behavior has not been achieved yet. Most of the investigations dealt with the quantitative analysis of the frequency and oscillator force behavior. Moreover, Raman-scattering data concerning the In-rich compositional range ($x>0.7$) remain scarce.[19]

In this paper we reconsider the issue of long-wavelength optical-phonon behavior in $Ga_{1-x}In_xAs$. We present a thorough Raman-scattering study, covering the whole compositional range and including the complete analysis of the optical-phonon frequencies, symmetries, and Raman intensities. Our purpose is to account for both the frequency and Raman intensity compositional dependencies of the long-wavelength TO and LO phonons in $Ga_{1-x}In_xAs$. To avoid turning this topic into a simple matter of fitting more parameters to more data, we attempt to account for our data with a model using solely parameters related to the two binary compounds.

Due to the original lattice mismatch ($\Delta r/r\approx 7\%$) between GaAs and InAs, structural disorder is superimposed to the chemical disorder in the alloy. Indeed, it is now well established from extended x-ray-absorption fine-structure spectroscopy (EXAFS),[20] that the original misfit is accommodated by local bond distortions (microscopic strains). It was shown that, despite this disorder, the concept of phonon dispersion still holds in alloys.[21–24] Finally, owing to the fact that the atoms carry dynamical charges, long-range Coulomb interactions have to be considered.

This paper is organized as follows. Our experimental results are presented in Sec. II. The whole compositional range is explored, and for each composition five different scattering configurations (at least) have been systematically used. Since only a very few results were available on alloys with high In contents, a particular attention is devoted to alloys with $0.7<x<1$. We shall show that the latter are important to achieve a clear understanding of the optical-phonon behavior.

The frequency behavior is analyzed in two steps. At first, in Sec. III, the behavior of the nonpolar TO is analyzed by

 © 1998 The American Physical Society

taking into account the mass disorder and the microscopic strains. Second, in Sec IV, we take into account the ionic character of the bonds in order to discuss the LO behavior: the long-range Coulomb interactions are shown to couple the GaAs- and InAs-like LO modes.

In Sec V, the Raman intensities are analyzed. The experimental data are compared with calculations performed within the frame of a dielectric model. Finally, the resulting optical mode behavior (frequencies and intensities) is discussed, and the main results are summarized in Sec. VI.

II. EXPERIMENTAL RESULTS

Raman spectroscopy measurements have been performed at room temperature on a large number of $Ga_{1-x}In_xAs$ layers, using a Dilor *XY* triple monochromator equipped with a liquid-N_2-cooled charge-coupled device (CCD) detector. Selective resonance effects were avoided since the spectra were excited with the 530.9-nm line of a Kr^+ laser. The corresponding energy indeed lies far from any specific electronic transition, whatever the alloy composition. Moreover, the corresponding Raman probing depth ranges from 30 ($x=1$) to 50 nm ($x=0$).

The layers were grown by molecular-beam epitaxy on GaAs or InP substrates. It is known that the misfit strain between the layer and substrate is relieved by plastic relaxation when the layer thickness exceeds a critical value. The effects of strain relaxation on the Raman scattering in thin $Ga_{1-x}In_xAs$ epilayers have been discussed in Ref. 19. Here, only completely relaxed $Ga_{1-x}In_xAs$ layers, with thicknesses in the μm range, were investigated. Moreover, by choosing a small Raman probing depth (i.e., probing the region close to the surface) one ensures that the Raman signals related to the structural defects (resulting from the plastic relaxation) are minimized.[19] We verified, for instance, that the Raman spectra of a thick relaxed $Ga_{0.47}In_{0.53}As$ layer grown on GaAs (-3.9% lattice mismatch) and a $Ga_{0.47}In_{0.53}As$ layer grown on InP (lattice matched) do not differ.

The spectra were recorded in the backscattering geometry. Two orientations of the substrate, [001] and [111], were systematically used. Moreover using a micro-Raman setup, spectra were also recorded on cleaved (110) surfaces. The corresponding long-wavelength TO and LO Raman selection rules in zinc-blende structures (Γ_{15} component of the Raman tensor) are reported in Table I.[25] In the backscattering geometry, whereas only LO scattering is expected for a (001) surface and TO scattering for a (110) surface, they are both allowed for a (111) surface. The spectra of GaAs ($x=0$) displayed in Fig. 1(a) show the benefit of using different surface orientations and polarizations of the incident and scattered electric fields for identifying the symmetries of the optical modes (see Table I).

A representative sampling of Raman spectra of $Ga_{1-x}In_xAs$ layers is shown in Figs. 1 and 2. At first glance, the first order optical range can be divided in two parts: lower- (217–240 cm^{-1}) and the upper-frequency (241–292 cm^{-1}) ones which are assigned to InAs- and GaAs-like optical modes, respectively. In each part, two types of features have in principle to be considered: those related to long-wavelength optical modes and those related to disorder-activated scattering.[3,26,27] LO features are seen in the (001) backscattering spectra. They can also be identified in the (111) backscattering spectra, if one compares the crossed and parallel polarization configurations (Table I). The TO features are expected to be the dominant ones in (110) backscattering spectra. Disorder-activated TO (DATO) features are also observed.

TABLE I. Raman selection rules (Γ_{15} component) in backscattering geometry on (001), (110), and (111) surfaces; **k** and **e** are the light wave vector and polarization, respectively. i stands for incident light and s for scattered light, with $x=[100]$, $y=[010]$, $z=[001]$, $x'=[1\bar{1}0]$, $y'=[110]$, $z'=[111]$ and $y''=[11\bar{2}]$. d_{TO} and d_{LO} are the TO and LO Raman tensor components, respectively.

	$k_i(e_i,e_s)k_s$	TO	LO
(001)	$z(x,y)\bar{z}$	0	$\lvert d_{LO}\rvert^2$
	$z(x,x)\bar{z}$	0	0
(111)	$z'(x',x')\bar{z}'$	$\frac{2}{3}\lvert d_{TO}\rvert^2$	$\frac{1}{3}\lvert d_{LO}\rvert^2$
	$z'(x',y'')\bar{z}'$	$\frac{2}{3}\lvert d_{TO}\rvert^2$	0
(110)	$y'(x',z)\bar{y}'$	$\lvert d_{TO}\rvert^2$	0
	$y'(z,z)\bar{y}'$	0	0

In Ga-rich layers, DATO appear just below the GaAs-like TO frequencies, as shown in Fig. 3. The DATO maximum lies close to the frequencies of the zone-edge TO phonons, as they are expected to mirror the optical-phonon density of states. The frequency splitting between the maximum of the GaAs-like DATO band and the TO peak indeed corresponds to the difference between the Brillouin-zone-center and edge TO frequencies in GaAs (≈ -9 cm^{-1}) see Fig. 3; The dispersion of the TO modes in bulk InAs is very weak: the frequencies of the zone-center and -edge TO modes differ only by ≈ -2 cm^{-1}.[28] Consequently, the InAs-like TO peak and DATO band are superimposed on the spectra (see Fig. 3). Our results are consistent with those reported in Ref. 16 on near-lattice-matched $Ga_{1-x}In_xAs$/InP ($0.48<x<0.58$; the peak labeled R^* in Ref. 16 corresponds to the GaAs-like DATO) and in Ref. 14 on $Ga_{0.47}In_{0.53}As$/InP(111). The long-wavelength TO modes observed in IR spectra[12,13] do correspond to our TO peaks (and not to the DATO ones). This supports the assignments we made.

It is worth mentioning that, in addition to DATO, we have also observed broad features related to disorder-activated acoustical modes (not shown here; see, for instance, Refs. 3, 17, and 26). The strength of all these disorder-activated features depends on the amount of disorder: they are weak in $Ga_{1-x}Al_xAs$ (chemical disorder) and strong in $Ga_{1-x}In_xAs$ (both chemical and structural disorder). Moreover, the DATO Raman selection rules do correspond to Γ_{15} symmetry, as expected.[29]

One may wonder whether there is evidence in our spectra for atomic ordering. It has been shown that Raman scattering provides valuable and qualitative information on atomic order in alloys (see, for instance, the investigation of long-range atomic ordering in $GaInP_2$ by means of Raman scat-

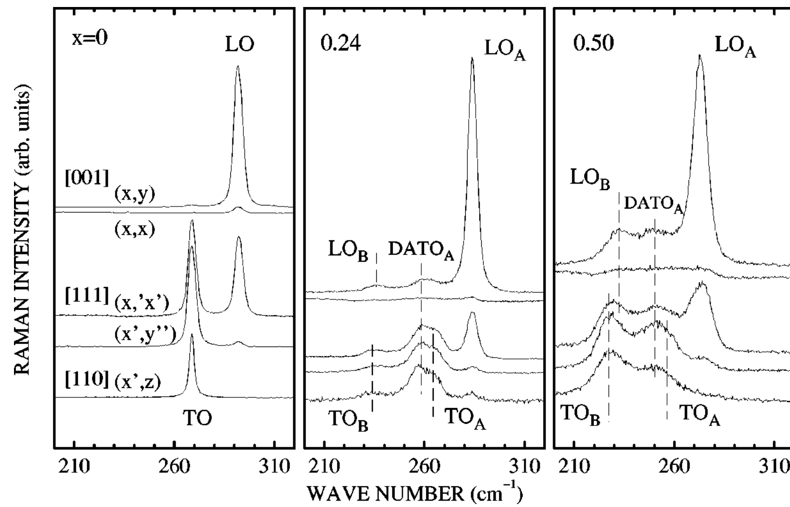

FIG. 1. $Ga_{1-x}In_xAs$ Raman spectra: $x=0$, 0.24, and 0.50. The [001], [111], and [110] surface orientations are indicated. The polarization configurations are given in parentheses. The subscripts A and B stand for GaAs- and InAs-like, respectively.

tering in Refs. 30 and 31). Long-range atomic order was shown to depend much on growth techniques and conditions (substrate temperature, orientation or misorientation, growth rates, and III/V ratio), and is usually shown by means of electron microscopy and diffraction techniques.[32–35]

According to electron microscopy measurements,[36] long-range atomic order is not present in our samples. Superlattice effects, like those observed in both the optical- and acoustical-phonon Raman spectra in Refs. 30 and 31, were not observed in the Raman spectra of our samples.

We have to mention that Mintairov and co-workers assigned the DATO features observed in the spectra recorded on (001) and (110) surfaces to additional LO and TO modes, respectively.[37,38] These authors attributed the corresponding three- and four-mode behaviors to the presence of long-range atomic order in their samples. The existence of ordered phases in their samples was, however, not demonstrated by means of other techniques.

We want to point out that the spectra recorded on various samples, obtained by means of different growth techniques (molecular beam epitaxy, metalorganic molecular beam epitaxy, liquid phase epitaxy, etc.), under different growth conditions and with different substrate orientations all display similar DATO bands. Moreover, when structural disorder is superimposed on the intrinsic alloy disorder (for instance, as a consequence of plastic relaxation in thin epilayers[19]), the intensity of the DATO features increases significantly. This corroborates they are unambiguously disorder activated features.

To summarize, both the GaAs- and InAs-like LO and TO peaks have been identified over the whole compositional range. Their frequencies are reported in Fig. 4. Whereas the TO frequencies evolve rather linearly with x, the GaAs- and InAs-like LO frequencies display positive and negative bowings, respectively. The impurity mode frequencies extrapolated from our data, $\omega_{\mathrm{GaAs:In}}=237\ \mathrm{cm}^{-1}$ and $\omega_{\mathrm{InAs:Ga}}=241\ \mathrm{cm}^{-1}$, are in good agreement with the values reported previously.[12,17] The ratio of the integrated GaAs- and InAs-like TO intensities scales almost like $(1-x)/x$. The LO intensities do obviously not follow this scaling law. Even when the Ga amount is as small as 5%, the GaAs-like LO intensity is as intense as the InAs-like one. Our purpose is now to

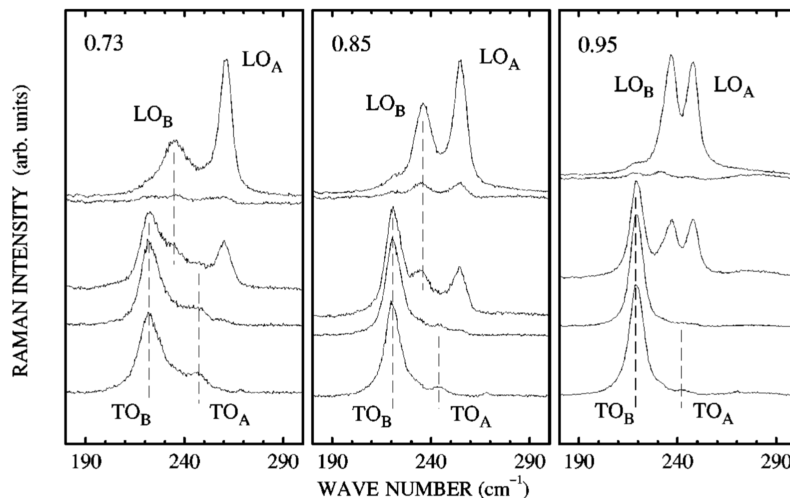

FIG. 2. $Ga_{1-x}In_xAs$ Raman spectra: $x=0.75$, 0.85, and 0.95. Notations are the same as in Fig. 1.

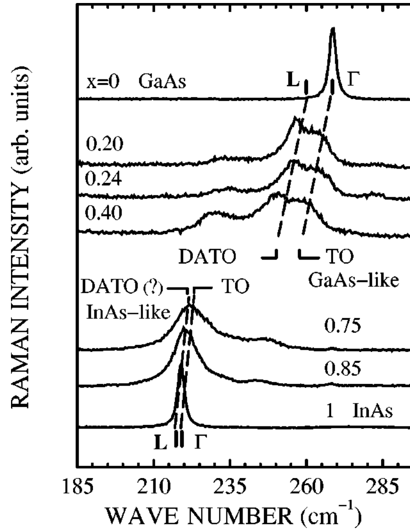

FIG. 3. Raman spectra recorded on (110) surfaces, displaying TO and DATO features. The Γ and L point TO frequencies in GaAs and InAs are indicated. The dashed lines are guides for the eye.

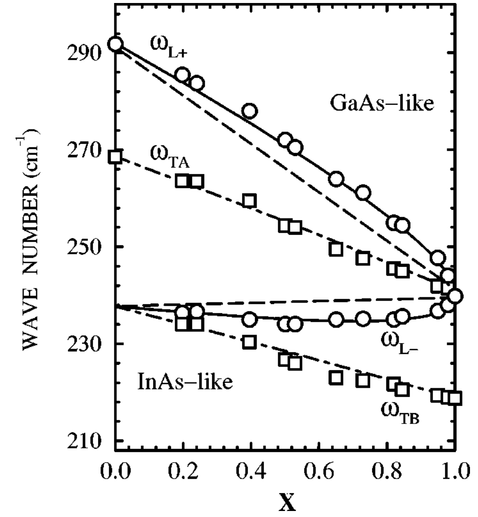

FIG. 4. Compositional dependencies of LO (circles) and TO (squares) frequencies. The solid lines are the calculated LO values: $\omega_{L,+}$ and $\omega_{L,-}$ are deduced from Eq. (14). The dot-dashed lines are the calculated TO values: $\omega_{T,A}$ and $\omega_{T,B}$ are deduced from the linear interpolation of the squared TO frequencies between their respective values for $x_i=0$ and 1. The dashed lines indicate the LO frequencies calculated disregarding coupling ($\sqrt{E_A}$ and $\sqrt{E_B}$).

account for the compositional dependencies of both the frequencies and Raman intensities of the optical modes in $Ga_{1-x}In_xAs$.

III. MASS DISORDER AND MICROSCOPIC STRAINS

In a binary material (AC or BC), the collective vibrations of all the harmonic oscillators are described in terms of phonons. The TO frequency is essentially determined by short-range interactions and can be written

$$\omega_T^2=\frac{K_T}{\mu}, \tag{1}$$

where μ is the reduced mass of the bonds and K_T an *effective* force constant. K_T accounts for both the mechanical interactions (between the nearest-neighbor atoms and others) and the Coulomb interaction due to the local part of the dynamical transverse charge.[1,39] In the materials we are concerned with, the contribution of this local part to K_T remains small.[13]

We shall describe the optical phonons in the $(AC)_{1-x}(BC)_x$ alloy by a set of effective AC- and BC-like oscillators (hereafter labeled A and B). Their relative number is defined by the alloy composition

$$x_A=1-x \quad \text{and} \quad x_B=x. \tag{2}$$

The labels A and B hence correspond to the GaAs and InAs oscillators, respectively. Each type of oscillator ($i=A$ or B) is characterized by its reduced mass (μ_i), its bond length (r_i), its effective force constant ($K_{T,i}$), and its dynamical charge ($e^*_{T,i}$).

As shown in Fig. 3, the TO Raman spectra in $Ga_{1-x}In_xAs$ display a two-mode behavior. The TO frequencies in pure GaAs and InAs differ significantly: 268.6 and 218.8 cm^{-1}, respectively. This difference is mainly due to the difference between their reduced masses. The latter difference is obviously preserved for the A and B oscillators in the alloy. Hence one expects the GaAs- and InAs-like characters to be preserved in the alloy. Indeed, when the optical frequencies of the AC and BC binary compounds differ significantly, the B (A) atoms are not expected to participate in AC-like (BC-like) vibrations. This is closely related to the phonon confinement in quantum wells or small particles.

The squared TO frequencies in $Ga_{1-x}In_xAs$, $\omega_{T,A}^2$ and $\omega_{T,B}^2$, are reported in Fig. 5(a). They both scale almost linearly with x. $\omega_{T,B}^2$ decreases when x_B decreases, whereas $\omega_{T,A}^2$ increases when x_A decreases. These dependencies can be explained as due to two effects: mass disorder and microscopic strains.[40] Mass disorder refers to the fact that when one is concerned with the response of the A oscillators, the B ones are at rest, and vice versa. Mass disorder lowers the phonon frequencies.[40] Compressive (tensile) microscopic strain increases (lowers) the phonon frequencies.

Obviously, depending on the local strain they experience or on the chemical nature of their neighbors, all the A (or B) oscillators are not equivalent. One may wonder whether or not, for a given type of oscillators (A or B), the different local configurations give rise to different Raman peaks. In fact, the corresponding frequency fluctuations are not large enough to produce any phonon localization (the criteria for phonon localization have been discussed in Ref. 41). Hence, the contributions of the A (B) oscillators give rise to a single peak, in a way similar to what occurs in isotopically disordered materials.[41–44] Both the mass disorder (mass) and microscopic strain (strain) effects can be viewed as a renormalization of the effective force constant. The squared frequency shift, relative to its value in the binary compound, is the sum of two contributions:[40,45]

$$\Delta\omega_{T,i}^2(x_i)=(\Delta\omega_{T,i}^2)_{\text{mass}}+(\Delta\omega_{T,i}^2)_{\text{strain}}. \tag{3}$$

We shall first discuss the GaAs-like TO frequency behavior in $Ga_{1-x}Al_xAs$, which is also reported in Fig 5(a). As local bond distortions are negligible in $Ga_{1-x}Al_xAs$, the ob-

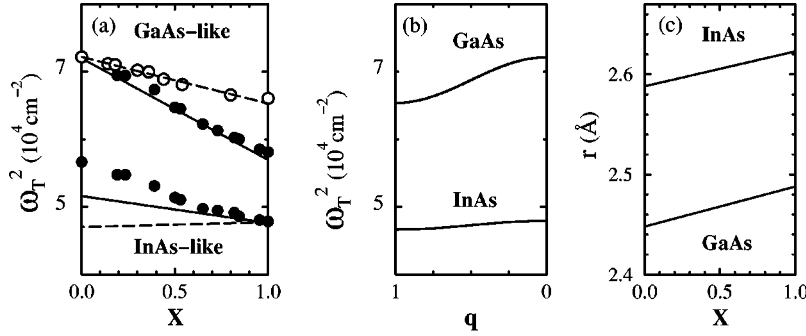

FIG. 5. (a) Schematic plot of the squared TO frequency dispersion (in the Γ-L direction) for GaAs and InAs. (b) Compositional dependencies of $\omega_{T,A}^2$ and $\omega_{T,B}^2$ in $Ga_{1-x}In_xAs$ (filled circles). The dashed lines refer to the mass-disorder-related downshift. The solid lines indicate the calculated dependencies (including both the mass disorder and microscopic strain terms). The open circles refer to the GaAs-like TO squared frequencies in $Ga_{1-x}Al_xAs$ (taken from Ref. 2 and our own data). (c) Schematic plot of the InAs and GaAs mean bond lengths in $Ga_{1-x}In_xAs$, as deduced from EXAFS measurements (Ref. 20).

served downshift is solely related to mass disorder. $\omega_{T,A}^2$ scales (almost) linearly with x_A. The vibrations of the GaAs-like modes are totally extended and localized in real space for $x_A=1$ and 0, respectively. The impurity mode frequency ($x_A=0$) lies close to the maximum of the GaAs TO density of states which corresponds to the frequencies of the L-point phonons in the Brillouin zone.[46] The observed downshift can therefore be linked to the GaAs TO dispersion [schematically reported in Fig. 5(b)].

We assume $(\Delta\omega_{T,A}^2)_{mass}$ to be the same in $Ga_{1-x}In_xAs$ and $Ga_{1-x}Al_xAs$. In $Ga_{1-x}Al_xAs$, the GaAs-like TO frequencies are located in the frequency gap between the optical and acoustical AlAs-like modes, and in $Ga_{1-x}In_xAs$ they lie above the InAs-like ones. In both systems the GaAs-like TO are thus well confined.

As all the available alloys based on InAs do imply local bond distortions, we shall simply estimate $(\Delta\omega_{T,B}^2)_{mass}$ from the maximum in the density of TO modes in InAs (following the discussion just above). Owing to the very weak InAs TO dispersion [see Fig. 5(b)], the effects of mass disorder on $\omega_{T,B}^2$ are expected to remain weak. The dashed lines in Fig 5(a) indicate the contributions to the compositional dependencies of $\omega_{T,A}^2$ and $\omega_{T,B}^2$ which are due to mass disorder.

Let us now consider the microscopic strain effects. The nearest neighbor bond lengths in $Ga_{1-x}In_xAs$ deduced from EXAFS (Ref. 20) are reported in Fig. 5(c) . The InAs and GaAs mean that bond lengths do not follow Vegard's law but remain rather close to their respective values in the unmixed binary materials.[47] The GaAs bonds are stretched and the InAs ones are compressed. The microscopic strain term in Eq. (3) is given by[48]

$$\frac{\Delta\omega_{T,i}^2}{\omega_{T,i}^2}=-6\gamma_i\left(\frac{\Delta r}{r}\right)_i, \tag{4}$$

where $(\Delta r/r)_i$ is the relative change in the bond lengths and γ_i the corresponding Grüneisen parameter.[49] The $BC{:}A$ impurity mode frequencies have been correctly predicted for several III-V alloys by considering the deformation of an AC_4 tetrahedron embedded in a BC matrix.[48,50,51] At any given composition x, the nearest-neighbor distances, as measured by EXAFS, are an average over different local arrangements in a macroscopic volume.[52] The AC-like (BC-like) TO mode also does experience a large set of local configurations, and its frequency shift therefore corresponds to the average distortion of the AC (BC) bonds. We have calculated the microscopic strain terms using $(\Delta r/r)_A(\%)=+1.6x_A$ and $(\Delta r/r)_B(\%)=-1.3x_B$ (according to Ref. 20), and the TO Grüneisen parameters of pure GaAs and InAs ($\gamma_{T,GaAs}=1.38$ and $\gamma_{T,InAs}=1.21$; Refs. 53 and 54). It is worth mentioning that the microscopic strain term in IV-IV alloys calculated by Rucker and Methfessel[40] by means of numerical calculations on one hand, and using Eq. (4) and the Grüneisen parameters of pure compounds on the other hand, coincide to within better than 10%.

The calculated compositional dependencies of $\omega_{T,A}^2$ and $\omega_{T,B}^2$ are reported in Fig 5(a). Our calculation accounts rather well for the observed compositional dependence of the GaAs-like TO frequencies. Concerning the InAs-like TO frequencies, the agreement is satisfactory for $0.6<x<1$. In the Ga-rich compositional range, the InAs-like modes are band modes: their frequencies overlap with the density of states of the GaAs-like optical modes.[17] One can therefore not expect our simple model to describe the InAs-like TO frequency behavior fully in the Ga-rich compositional range.

It is interesting to consider the InAs-like TO modes in $InAs_xP_{1-x}$; they are true gap modes, as their frequencies lie well within the gap between the optical and acoustical modes of InP.[7] Our calculation [using $(\Delta r/r)_B(\%)=-0.9x_B$ (Ref. 55)] yields $-8.7x_B$ and $+31x_B$ (in 10^2 cm^{-2}) for the mass disorder and microscopic strain terms, respectively. The sum thus yields $+22.3x_B$ (in 10^2 cm^{-2}) and compares well with experiment: $+22.1x_B$ (in 10^2 cm^{-2}).

To summarize, the TO frequency behavior is rather well accounted for. For the GaAs-like TO mode, the mass disorder and microscopic strain terms have the same sign, resulting in the observed strong downshift of $\omega_{T,A}^2$ when x_A decreases. For the InAs-like TO mode, on the contrary, these terms have opposite signs and thus partially compensate for one another. However, as the mass-disorder-related shift remains weak, the changes are essentially related to the compressive strains (which are higher in $Ga_{1-x}In_xAs$ than in $InAs_{1-x}P_x$). The latter account for the increase of $\omega_{T,B}^2$ when x_B decreases.

IV. IONIC PLASMON COUPLING

A. In an alloy

In order to discuss the LO frequency behavior, we shall now include the long-range effects related to the effective transverse charges e_T^*. We are concerned with dynamical charges; they include a static part which moves rigidly with the atomic core, and a dynamical contribution which arises from the redistribution of the charges as a result of the motion of these cores.[56] They are microscopic parameters which refer to atoms.[25,56]

Let us first consider a binary polar material. In a cubic crystal, the short-range restoring forces K_T are the same for LO and TO modes. However, only LO displacements u_L produce a macroscopic ionic polarization. The corresponding macroscopic electric field E_L produces an additional restoring force, and gives rise to the LO-TO splitting[25]

$$-\omega_L^2 u_L = -\omega_T^2 u_L + \frac{e_T^*}{\mu} E_L . \tag{5}$$

The ionic plasmon frequency Ω_p is given by

$$\Omega_p^2 = \omega_L^2 - \omega_T^2 = \frac{N e_T^{*2}}{\mu \varepsilon_0 \varepsilon_\infty} \tag{6}$$

(ε_0 is the permittivity of vacuum and ε_∞ the high frequency value of the dielectric function).

In the $A_{1-x}B_xC$ alloy, one has to consider the dynamical transverse charges $e_{T,A}^*$ and $e_{T,B}^*$ of the A and B oscillators. These oscillators contribute to the same ionic polarization:

$$\begin{aligned} P_{ion} &= N x_A e_{T,A}^* u_{L,A} + N x_B e_{T,B}^* u_{L,B} \\ &= -\varepsilon_0 \varepsilon_\infty(x)\, E_L , \end{aligned} \tag{7}$$

where $\varepsilon_\infty(x)$ is the high-frequency value of the dielectric function of the alloy. Consequently, the two types of oscillators are coupled by the macroscopic electric field:

$$\begin{aligned} -\omega^2 u_{L,A} = -\omega_{T,A}^2 u_{L,A} - \frac{N e_{T,A}^*}{\mu_A \varepsilon_0 \varepsilon_\infty(x)} \\ \times (x_A e_{T,A}^* u_{L,A} + x_B e_{T,B}^* u_{L,B}), \end{aligned} \tag{8}$$

$$\begin{aligned} -\omega^2 u_{L,B} = -\omega_{T,B}^2 u_{L,B} - \frac{N e_{T,B}^*}{\mu_B \varepsilon_0 \varepsilon_\infty(x)} \\ \times (x_A e_{T,A}^* u_{L,A} + x_B e_{T,B}^* u_{L,B}). \end{aligned} \tag{9}$$

Defining normal coordinates by $Q_A = \sqrt{\mu_A N_A}\, u_{L,A}$ and $Q_B = \sqrt{\mu_B N_B}\, u_{L,B}$, the eigenvalues and eigenmodes for LO modes then appear as solutions of a coupled two-level system:

$$\begin{pmatrix} E_A - E & V_{AB} \\ V_{AB} & E_B - E \end{pmatrix} \begin{pmatrix} Q_A \\ Q_B \end{pmatrix} = 0, \tag{10}$$

$$V_{AB} = \Omega_{p,A}(x_A)\, \Omega_{p,B}(x_B), \tag{11}$$

$$E_i = \omega_{T,i}^2 + \Omega_{p,i}^2(x_i), \tag{12}$$

$$\Omega_{p,i}^2(x_i) = x_i \frac{\varepsilon_{\infty,i}}{\varepsilon_\infty(x)} (\omega_{L,i}^2 - \omega_{T,i}^2), \tag{13}$$

with $i = A$ or B.

E_A and E_B are the energy levels before coupling; they scale almost linearly with x. In a schematic picture, one may consider that short-range effects (mass disorder and bond distortions) and long-range effects (dynamical charges) are included in $\omega_{T,i}^2$ and $\Omega_{p,i}^2$, respectively. The coupling parameter V_{AB} depends on the ionic plasmon frequencies, $\Omega_{p,i}(x_i)$. The squared ionic plasmon frequency of the binary material $\omega_{L,i}^2 - \omega_{T,i}^2$ is weighted by the number of oscillators i, and supports a screening effect $[\varepsilon_{\infty,i}/\varepsilon_\infty(x)]$.

The LO frequencies can be easily deduced from the eigenvalues $E_\pm = \omega_{L\pm}^2$ of Eq. (10),

$$E_\pm = \bar{E}_{AB} \pm \sqrt{\Delta_{AB}^2 + V_{AB}^2}, \tag{14}$$

with

$$\bar{E}_{AB} = \frac{E_A + E_B}{2} \quad \text{and} \quad \Delta_{AB} = \frac{E_A - E_B}{2}. \tag{15}$$

The eigenvectors can be written as

$$|Q_+\rangle = \cos\theta\,|Q_A\rangle + \sin\theta\,|Q_B\rangle, \tag{16}$$

$$|Q_-\rangle = \cos\theta\,|Q_B\rangle - \sin\theta\,|Q_A\rangle, \tag{17}$$

where θ is given by

$$\tan(2\theta) = \frac{V_{AB}}{\Delta_{AB}}. \tag{18}$$

The degree of mixing is given by $\tau = |\tan\theta|^2$. The pure A and B characters are only preserved for $x = 0$ and 1.

The coupling between the LO modes is reinforced when either the coupling parameter V_{AB} increases, or the energy gap Δ_{AB} decreases. Hence, the higher the ratio value V_{AB}/Δ_{AB} is, the more strongly the GaAs- and InAs-like LO frequencies repel each other, and the more the A and B displacements are mixed.

It is worth noting that the LO frequencies $\omega_{L\pm}(x)$ deduced from Eq. (10) coincide with the zeros of the mean dielectric function defined by

$$\varepsilon(\omega,x) = (1-x)\varepsilon_A(\omega,x) + x\varepsilon_B(\omega,x). \tag{19}$$

The latter can be written as (including the phenomenological damping constant Γ_i)

$$\varepsilon(\omega,x) = \varepsilon_\infty(x)\left(1 + \sum_{i=A,B} \frac{\Omega_{p,i}^2(x_i)}{\omega_{T,i}^2 - \omega^2 - \mathbf{i}\omega\Gamma_i}\right), \tag{20}$$

with

$$\varepsilon_\infty(x) = (1-x)\varepsilon_{\infty,A} + x\varepsilon_{\infty,B} . \tag{21}$$

The coupling effects will be discussed within the frame of the dielectric model in Sec. V.

TABLE II. Parameters used in the calculations. Frequencies are given in cm^{-1}.

	ω_L	ω_T	$\omega_{impurity}$	ε_∞[a]
InAs	239.8	218.8	237.7	12.3
GaAs	291.9	268.6	241	10.9

[a]Reference 46.

B. In $Ga_{1-x}In_xAs$

We now apply the model to $Ga_{1-x}In_xAs$. E_A, E_B, and V_{AB} depending on x, according to Eqs. (11)–(13). As discussed in Sec. III, mass disorder and bond distortions affect the short-range restoring forces $K_{T,i}$, and hence $\omega_{T,i}^2$. The linear dependence of $\omega_{T,A}^2$ and $\omega_{T,B}^2$ on x (between their respective binary material and impurity mode values) has been accounted for in the calculation of E_A and E_B.

It is known that strain may also modify e_T^* (see, for instance, Refs. 53, 54, and 56). The TO and LO Grüneisen parameters indeed differ: $\gamma_{T,GaAs}=1.38$, $\gamma_{L,GaAs}=1.23$, $\gamma_{T,InAs}=1.21$, and $\gamma_{L,InAs}=1.06$.[53,54] The changes of $e_{T,i}^2$ (i.e., $\omega_{L,i}^2-\omega_{T,i}^2$) due to the local bond distortions have also been included in the calculations. However, they remain weak: they do not exceed +2.7% for GaAs and −1.7% for InAs. If one excepts these very small corrections, we have assumed that the dynamical charges $e_{T,A}^*$ and $e_{T,B}^*$ do not depend on composition. The values used in the calculations are reported in Table II. $\varepsilon_\infty(x)$ has been calculated according to Eq. (21).

The compositional dependencies of Δ_{AB}, V_{AB}, and V_{AB}/Δ_{AB} in $Ga_{1-x}In_xAs$ are reported in Figs. 6(a) and 6(b). V_{AB} reaches its maximum value in the middle of the compositional range, and vanishes at $x=0$ and 1. Δ_{AB} decreases rapidly with increasing x, and becomes even smaller than V_{AB}. Strong coupling occurs when $V_{AB}/\Delta_{AB}>1$. The compositional dependencies of $\cos^2\theta$ and $\sin^2\theta$ are reported in Fig. 6(c). The mixing between the A and B characters is important in the In-rich compositional range; τ reaches 60% for $x=0.98$. The upper (lower) frequency mode $|Q_+\rangle$ ($|Q_-\rangle$), however, always preserves its GaAs (InAs) dominant character.

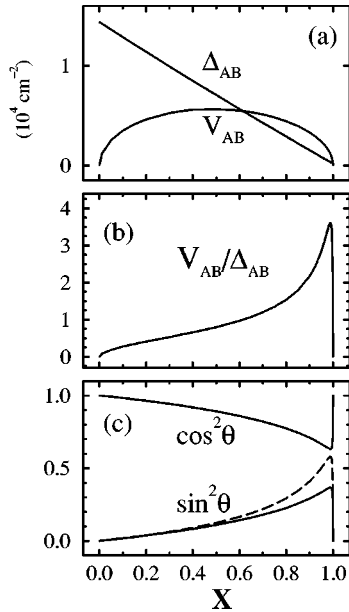

FIG. 6. Compositional dependencies of (a) Δ_{AB} and V_{AB}, (b) V_{AB}/Δ_{AB}, and (c) $\cos^2\theta$ and $\sin^2\theta$. The dashed line in (c) indicates the degree of mixing τ.

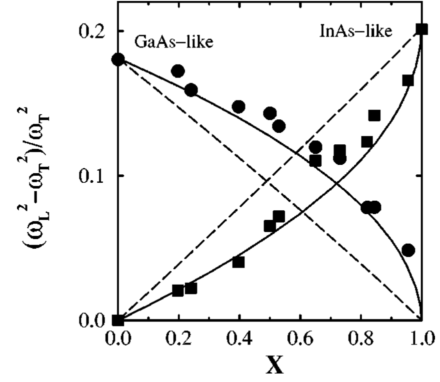

FIG. 7. Compositional dependencies of $(\omega_{L,+}^2-\omega_{T,A}^2)/\omega_{T,A}^2$ and $(\omega_{L,-}^2-\omega_{T,B}^2)/\omega_{T,B}^2$: experiment (circles and squares, respectively) and calculation with coupling (solid line) and without coupling (dashed line).

The GaAs- and InAs-like LO frequencies (i.e., $\sqrt{E_+}$ and $\sqrt{E_-}$) are reported in Fig. 4 (solid lines). The calculated frequencies are in good agreement with the experimental data over the whole range of composition. No adjustable parameters have been used in the calculation. The LO frequencies obtained when disregarding coupling, i.e., $\sqrt{E_A}$ and $\sqrt{E_B}$, are also reported (dashed lines). Due to the coupling, the GaAs- and InAs-like LO frequencies repel each other. Hence the GaAs-like LO-TO splitting (upper frequency oscillator) is increased and the InAs-like LO-TO splitting (lower frequency oscillator) is decreased. The bowing of LO-like frequencies is well accounted for by the calculation. The strong coupling mainly originates in the small gap between $\sqrt{E_A}$ and $\sqrt{E_B}$ (dashed lines). The strong coupling (Fig. 6) accounts for the persistence of a high value of the GaAs-like TO-LO splitting in In-rich samples. At the impurity limit for a given oscillator ($i=A$ or B), the LO-TO splitting vanishes, since $x_i=0$ (and not because $e_{T,i}^*$ vanishes, as stated in Ref. 57).

Let us now discuss the oscillator strength (S) behavior. For binary material, S_i is given by

$$S_i=\varepsilon_{\infty,i}\frac{\omega_{L,i}^2-\omega_{T,i}^2}{\omega_{T,i}^2}, \qquad (22)$$

and is hence proportional to $e_{T,i}^{*2}$ [Eq. (6)]. The compositional dependences of $(\omega_{L,+}^2-\omega_{T,A}^2)/\omega_{T,A}^2$ and $(\omega_{L,-}^2-\omega_{T,B}^2)/\omega_{T,B}^2$ are shown in Fig. 7. Our calculation compares well with the experimental data. The coupling causes oscillator strength transfer, as shown by the bowing with respect to the dashed lines in Fig. 7 (calculated disregarding coupling, i.e., setting $V_{AB}=0$). S_+ is increased to the detriment of S_-. The A and B contributions to the ionic polarization field are in phase for the upper frequency LO mode and in antiphase for the lower-frequency one.[15]

We have assumed that the dynamical charges $e^*_{T,A}$ and $e^*_{T,B}$ do not depend on composition (excepting the very small changes due to the microscopic strains). Good agreement with the experimental data (Figs. 4 and 7) has been obtained within this assumption. Hence, unlike what was inferred in Refs. 17 and 58, the oscillator strength transfer is not related to dynamical charge transfer (from the In to Ga ions). One indeed has to keep in mind that, due to the coupling and mixing (Fig. 6), S_+ cannot be assigned solely to the A oscillators, and S_- to the B oscillators. In particular, the upper (lower) frequency oscillator strength is not proportional to $e^{*2}_{T,A}$ ($e^{*2}_{T,B}$). According to our calculations, the LO frequency and oscillator strength behaviors are governed by the coupling effects.

V. RAMAN INTENSITIES

A. In an alloy

We calculate the Raman spectra within the framework of the dielectric model developed by Hon and Faust to account for Raman scattering by coupled LO-plasmon modes in doped semiconductors.[59] In our case, the Raman response is due to the electronic susceptibility modulation by the relative displacements u_A and u_B (deformation potential coupling) and the macroscopic electric field E (electro-optic coupling). Following the notations of Ref. 59, these three types of modulations are noted R_i ($R_1=E$, $R_2=u_A$, and $R_3=u_B$) and the corresponding susceptibility derivatives d_i. The Raman cross section is given by[59]

$$I(\omega)\propto\sum_{i=1}^{3}\sum_{j=1}^{3} d_i d_j \langle R_i R_j\rangle_\omega, \qquad (23)$$

where the brackets describe thermal power density. The fluctuation-dissipation theorem allows the determination of the spectral densities

$$\langle R_i R_j\rangle_\omega=\frac{h}{2\pi}[n(\omega,T)+1]\mathrm{Im}\{\alpha_{ij}\}, \qquad (24)$$

where $n(\omega,T)$ is the Bose population factor, and α_{ij} the matrix elements of the generalized Nyquist susceptibility defined by

$$R_i=\sum_{j=1}^{3}\alpha_{ij}F_j. \qquad (25)$$

F_j are generalized forces, F_1 is the free polarization field, and F_2 and F_3 are the mechanical forces acting on oscillators A and B, respectively. The α_{ij} matrix elements are deduced from the following set of equations:

$$-N_A e^*_{T,A}u_A-N_B e^*_{T,B}u_B-\varepsilon_0\varepsilon_\infty E=F_1, \qquad (26)$$

$$\mu_A\ddot{u}_A+\mu_A\gamma_A\dot{u}_A+\mu_A\omega^2_{T,A}u_A-e^*_{T,A}E=F_2/N_A, \qquad (27)$$

$$\mu_B\ddot{u}_B+\mu_B\gamma_B\dot{u}_B+\mu_B\omega^2_{T,B}u_B-e^*_{T,B}E=F_3/N_B, \qquad (28)$$

where $N_i=Nx_i$; ε_∞ accounts for the high-frequency electronic response. We factor out d_E^2 in Eq. (23) when calculating the Raman cross sections. The ratio between the electric field and atomic displacement modulations is given by ($i=A$ or B)

$$\frac{d_{u,i}}{d_E}=\frac{\mu_i\omega^2_{T,i}}{e^*_{T,i}}C_i, \qquad (29)$$

with

$$C_i=x_iC_i^0, \qquad (30)$$

where C_i^0 is the Faust-Henry coefficient of the binary material i. For the Raman scattering by LO modes, one finally obtains

$$I_L(\omega)\propto[n(\omega)+1]\mathrm{Im}\left\{-\frac{1}{\varepsilon(\omega,x)}\left[1+\left(2C_A-C_A^2\frac{\omega^2_{T,A}}{\Omega^2_{pl,A}}\right)\mathcal{L}_A+\left(2C_B-C_B^2\frac{\omega^2_{T,B}}{\Omega^2_{pl,B}}\right)\mathcal{L}_B-\left(2C_AC_B+\frac{\Omega^2_{pl,B}\,\omega^2_{T,A}}{\Omega^2_{pl,A}\,\omega^2_{T,B}}C_A^2+\frac{\Omega^2_{pl,A}\,\omega^2_{T,B}}{\Omega^2_{pl,B}\,\omega^2_{T,A}}C_B^2\right)\mathcal{L}_A\mathcal{L}_B\right]\right\}, \qquad (31)$$

where $\varepsilon(\omega,x)$ is the dielectric function defined by Eq. (20), and $\Omega^2_{pl,i}$ depends on x_i according to Eq. (13). $\mathcal{L}_i$ is the normalized Lorentzian response of an oscillator: $\mathcal{L}_i=(1-\omega^2/\omega^2_{T,i}-i\Gamma\omega/\omega^2_{T,i})^{-1}$. For TO phonons, a polariton term $(kc/\omega)^2$ has to be included in Eq. (26). Because of this term, in backscattering geometry ($k\gg\omega_T/c$) the contributions to the TO Raman intensities due to $\langle E^2\rangle_\omega$, $\langle Eu_A\rangle_\omega$, and $\langle Eu_B\rangle_\omega$ can be disregarded.[59] Consequently, one obtains

$$I_T\propto[n(\omega)+1]\mathrm{Im}\left\{C_A^2\frac{\omega^2_{T,A}}{\Omega^2_{pl,A}}\mathcal{L}_A+C_B^2\frac{\omega^2_{T,A}}{\Omega^2_{pl,A}}\mathcal{L}_B\right\}. \qquad (32)$$

B. In $Ga_{1-x}In_xAs$

The calculations were performed using the parameters reported in Table II. The Faust-Henry coefficients of GaAs and InAs are $C^0_{GaAs}=-0.55$ and $C^0_{InAs}=-0.53$.[60,61] Once again, a linear interpolation for $\omega^2_{T,A}$ and $\omega^2_{T,B}$ between their respective values in the binary materials has been used in order to account for the effects of mass disorder and bond distortions. The changes of $e^2_{T,i}$ (i.e., $\omega^2_{L,i}-\omega^2_{T,i}$) due to the local bond distortions were included in the calculations. Notice that, unlike the TO frequencies, the LO frequencies for $0<x<1$ are not input parameters but are derived from our model.

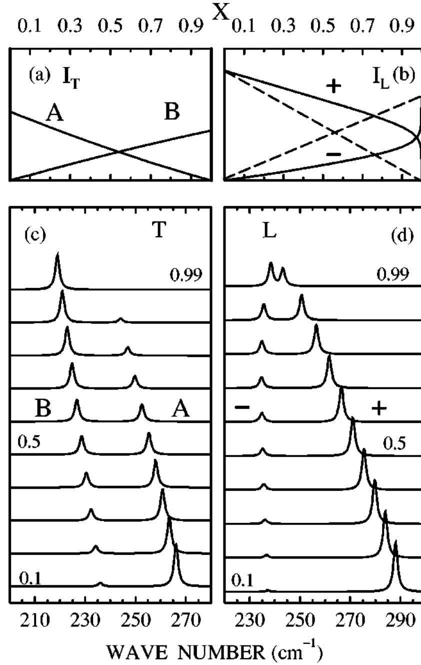

FIG. 8. Calculated (a) TO and (b) LO peak intensities. The dashed lines in (b) indicate the behavior expected in an uncoupled scheme. Calculated (c) TO and (d) LO Raman spectra: the compositions are (from bottom to top) $x=0.1$, 0.2, 0.3, 0.4, 0.5, 0.6, 0.7, 0.8, 0.9, and 0.99. Intensities are given in arbitrary units.

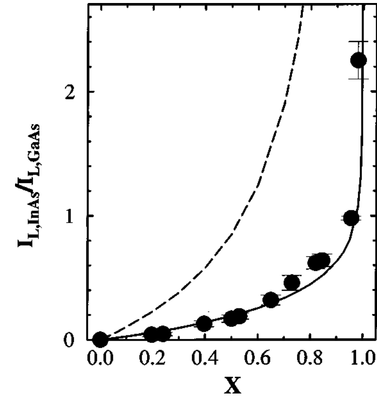

FIG. 9. InAs-like/GaAs-like LO intensity ratio: experiment (dots) and calculation with coupling (solid line) and without coupling (dashed line).

The LO and TO spectra calculated according to Eqs. (31) and (32) are reported in Fig. 8. Unlike the TO intensities, the LO ones do not scale linearly with x (Fig. 8).

The factor $\mathrm{Im}\{1/\varepsilon(\omega)\}$ contains the resonant effects for LO modes: resonances are maxima of $\langle E^2\rangle_\omega$.[59] Interference effects which are included in the term in brackets in Eq. (31) play only a minor role here. Due to the small phonon line broadening (a few cm^{-1}) and the gap between $\omega_{T,A}^2$ and $\omega_{T,B}^2$ which is preserved over the whole compositional range [Fig. 5(a)], the overlapping between the two spectral responses $\mathcal{L}_\mathcal{A}$ and $\mathcal{L}_\mathcal{B}$ of the oscillators remains very weak.[62] Consequently, the LO spectra calculated neglecting the interference term [i.e., using $I_L \propto \mathrm{Im}\{1/\varepsilon(\omega)\}$] instead of Eq. (31) are similar to the ones reported in Fig. 8. In particular, the frequencies of the LO response maximums in Eq. (31) coincide with the frequencies reported in Fig. 4.

In order to compare our model with our experimental data, we now consider the ratio between the GaAs and InAs-like LO intensities, $I_{L,InAs}/I_{L,GaAs}$. The intensity ratio calculated with (full line) and without coupling (dashed line) are reported in Fig. 9. The agreement between the model of coupled oscillators (full line) and the experimental data (dots) is very good over the whole compositional range. The upper frequency oscillator (which coincides with the symmetrical mode in the two-level scheme) supports the highest efficiency for modulating the electronic polarizability. One observes the reinforcement of the GaAs-like oscillator intensity to the detriment of the InAs-like one. The GaAs-like LO intensity remains higher than the InAs-like LO one, until x exceeds 0.98. The peculiar Raman intensity behavior in $Ga_{1-x}In_xAs$ is now accounted for. The intensity transfer originates in the coupling of the GaAs- and InAs-like oscillators. One deals unambiguously with a two-mode behavior.

It is not straightforward to compare the calculated TO spectra with the experimental data. The Raman spectra recorded on (110) or (111) surfaces display indeed strong DATO features. Hence the long-wavelength TO contributions cannot always be identified with a good accuracy. In particular, the InAs DATO and long-wavelength TO features are superimposed due to the weak TO dispersion. Nevertheless, one can verify that the integrated intensities of the TO-related features (TO+DATO) scale almost linearly with x.

Simulations of Raman spectra of doped and undoped alloys were previously reported by Mintairov and co-workers.[37,38,63] These authors used a molecular model of the electronic polarizability in the alloy, which is equivalent to the model we present here. The frequencies deduced for a given composition from the experimental Raman spectra were systematically used as input parameters in their model. We have shown how this can be avoided, and how the Raman spectra can be predicted whatever the composition.

VI. DISCUSSION AND CONCLUSION

We have presented a simple model which describes the optical-phonon behavior in $Ga_{1-x}In_xAs$. We have shown how the optical-phonon frequency and Raman intensity behavior can be derived from a small set of parameters. In addition to parameters related to the end-member crystals, one solely requires the impurity mode frequencies. The latter can also be estimated (with a satisfactory accuracy) from the end-member crystal characteristics [phonon dispersions, Grüneisen parameters, and lattice constants (Sec. III)]. We have intentionally avoided any fit to our experimental data. Hence the model presented here is able to predict the optical phonon behavior in alloys. It has been shown that the optical-phonon behavior results from three main effects: (i) mass disorder, (ii) microscopic strains, and (iii) coupling by the ionic polarization field.

The TO behavior is essentially determined by local effects (i) and (ii) (similarly to what occurs for optical phonons in covalent IV-IV materials[40,45]). Owing to their frequency gap, the InAs- and GaAs-like characters of the TO modes are preserved. The frequency shifts due to (i) can be estimated from the TO dispersion curves. The microscopic strains systematically reduce the frequency gap: the upper- (lower-) frequency mode experiences tensile (compressive) strain

which lowers (increases) its frequency.

Striking similarities exist between the TO frequency scheme [Fig. 5(a)] and the bond scheme obtained by EXAFS [Fig. 5(c).] The InAs and GaAs mean bond lengths also exhibit a bimodal or two mode behavior: they are close to their respective values in the binary materials and do not obey Vegard's law (see Ref. 47). This suggests that Raman scattering can be used as a reliable probe for local bond distortions in alloys.

To account for the LO behavior, one has to consider coupling (iii) by the long-range ionic polarization field, in addition to (i) and (ii). Unlike (i) and (ii), (iii) cannot be treated as a perturbation. We have proposed a simple model (coupled two-level system) which accounts for the observed nonlinear behavior of the LO frequencies and Raman intensities. Strong coupling occurs when GaAs- and InAs-like LO frequencies are or become close. Microscopic strains lead to a systematic reinforcement of the LO coupling, as they reduce the frequency gap. The oscillator strength and intensity are reinforced for the upper frequency mode (symmetric state—in phase), whereas they are screened for the lower-frequency mode (antisymmetric state—out of phase). The relative changes in the oscillator strength or Raman intensities are much larger than the relative frequency shifts. In the light of the present work, it is shown that dynamical charge transfer (which is obviously likely to occur) does not govern the optical phonon behavior (unlike it has been inferred in previous works[17,58]). It is important to notice that, due to the mixing, the LO modes cannot be assigned to a given oscillator, and hence to a given transverse effective charge.

One deals unambiguously with a two-mode behavior in $Ga_{1-x}In_xAs$ for both the TO and LO frequencies. Concerning their Raman intensities, the departures from the typical two-mode behavior in $Ga_{1-x}In_xAs$ can be explained as follows. (i) It is due to the LO coupling by the ionic plasmons; this coupling is very strong in In-rich samples and causes important mixing. (ii) For low In contents, the InAs-like modes are band modes; this may explain why InAs-like features are hardly detected and resolved in the Raman or IR spectra of Ga-rich samples.

Raman scattering provides obviously interesting information on electron-phonon interactions in alloys. From both practical and fundamental points of view, electron-phonon interactions are of particular interest; they have to be considered in transport measurements, phonon-assisted luminescence or tunneling, cyclotron resonance, etc., see, for instance, Ref. 15 and references therein. In particular, due to the coupling effects discussed here, one expects the Fröhlich coupling to InAs-like modes to be much weaker than to GaAs-like modes.[15] This can be demonstrated by means of Raman scattering. The resonant Raman-scattering measurements we performed (not reported here) on $Ga_{0.95}In_{0.05}As$ in the vicinity of the E_1 transition do show that the GaAs-like LO Fröhlich coupling constant is indeed larger than the InAs-like LO one.

The model we applied to $Ga_{1-x}In_xAs$ can obviously be extended to other $A_{1-x}B_xC$ alloys. For instance, the LO one mode behavior in $Ga_{1-x}Al_xN$ has been accounted for recently within the frame of the dielectric model presented here.[11] The optical-phonon behavior can be predicted by simply considering physical parameters of the end-member crystals. Even if some complexities of real systems have not been considered, the model presented here captures real and simple effects.

[1] M. Ilegems and G. I. Pearson, Phys. Rev. B **1**, 1576 (1970).
[2] O. K. Kim and W. G. Spitzer, J. Appl. Phys. **50**, 4362 (1979).
[3] B. Jusserand and J. Sapriel, Phys. Rev. B **24**, 7194 (1981).
[4] G. Lucovsky, K. Y. Cheng, and G. L. Pearson, Phys. Rev. B **12**, 4135 (1975).
[5] R. Ferrini, M. Galli, G. Guizzetti, M. Patrini, A. Bosacchi, S. Franchi, and R. Magnanini, Phys. Rev. B **56**, 7549 (1997).
[6] N. P. Kekelidze, G. P. Kekelidze, and Z. D. Makharadze, J. Phys. Chem. Solids **34**, 2117 (1973).
[7] R. Carles, N. Saint-Cricq, J. B. Renucci, and R. J. Nicholas, J. Phys. C **13**, 899 (1980).
[8] S. Emura, T. Nakagawa, S. Gonda, and S. Shimizu, J. Appl. Phys. **62**, 4632 (1987).
[9] L. Pavesi, R. Houdré, and P. Giannozzi, J. Appl. Phys. **78**, 470 (1995).
[10] B. Jusserand and S. Slempkes, Solid State Commun. **49**, (1984).
[11] F. Demangeot, J. Groenen, J. Frandon, M. A. Renucci, O. Briot, S. Clur, and R. L. Aulombard, Appl. Phys. Lett. **72**, 2674 (1998).
[12] M. H. Brodsky and G. Luckovsky, Phys. Rev. Lett. **21**, 990 (1968).
[13] S. Yamazaki, A. Ushirokawa, and T. Katoda, J. Appl. Phys. **51**, 3722 (1980).
[14] T. P. Pearsall, R. Carles, and J. C. Portal, Appl. Phys. Lett. **42**, 436 (1983).
[15] K. J. Nash, M. S. Skolnick, and S. J. Bass, Semicond. Sci. Technol. **2**, 329 (1987).
[16] J. P. Estrera, P. D. Stevens, R. Glosser, W. M. Duncan, Y. C. Kao, H. Y. Liu, and E. A. Beam III, Appl. Phys. Lett. **61**, 1927 (1992).
[17] G. Landa, R. Carles, and J. B. Renucci, Solid State Commun. **86**, 351 (1993).
[18] F. Calle, A. Sacedón, A. L. Alverez, E. Calleja, E. Muno, H. G. Colson, and P. Kidd, Microelectron. J. **26**, 821 (1995).
[19] J. Groenen, G. Landa, R. Carles, P. S. Pizani, and M. Gendry, J. Appl. Phys. **82**, 803 (1997).
[20] J. C. Mikkelsen and J. B. Boyce, Phys. Rev. Lett. **49**, 1412 (1982); Phys. Rev. B **28**, 7130 (1983).
[21] J. A. Kash, J. M. Hvam, J. C. Tsang, and T. F. Kuech, Phys. Rev. B **38**, 5776 (1988).
[22] B. Jusserand, D. Paquet, and F. Mollot, Phys. Rev. Lett. **63**, 2397 (1989).
[23] S. Baroni, S. de Gironcoli, and P. Giannozzi, Phys. Rev. Lett. **65**, 84 (1990).
[24] E. Molinari, in *Confined Electrons and Photons*, edited by E. Burstein and C. Weisbuch (Plenum, New York, 1995), and references therein.
[25] P. Y. Yu and M. Cardona, in *Fundamentals of Semiconductors* (Springer-Verlag, Berlin, 1996).
[26] E. Bedel, R. Carles, A. Zwick, J. B. Renucci, and M. A. Renucci, Phys. Rev. B **30**, 5923 (1984).

[27] O. Brafman and R. Manor, Phys. Rev. B **51**, 6940 (1995), and references therein.
[28] R. Carles, N. Saint-Cricq, J. B. Renucci, M. A. Renucci, and A. Zwick, Phys. Rev. B **22**, 4804 (1980).
[29] P. Etchegoin, H. D. Fuchs, J. Weber, M. Cardona, L. Pintschovius, N. Pyka, K. Itoh, and E. E. Haller, Phys. Rev. B **48**, 12 661 (1993).
[30] F. Alsina, N. Mestres, J. Pascual, C. Geng, P. Ernst, and F. Scholz, Phys. Rev. B **53**, 12 994 (1996).
[31] A. Hassine, J. Sapriel, P. Le Berre, M. A. Di Forte-Poisson, F. Alexandre, and M. Quillec, Phys. Rev. B **54**, 2728 (1996).
[32] T. S. Kuan, T. F. Kuech, W. I. Wang, and E. L. Wilkie, Phys. Rev. Lett. **54**, 201 (1985).
[33] M. A. Shahid, S. Mahajan, D. E. Laughlin, and H. M. Cox, Phys. Rev. Lett. **58**, 2567 (1987).
[34] A. Gomyo, T. Suzuki, and S. Iijima, Phys. Rev. Lett. **60**, 2645 (1988).
[35] A. Zunger and S. Mahajan, in *Handbook of Semiconductors*, 2nd ed., edited by S. Mahajan (Elsevier, Amsterdam, 1994), Vol. 3, p. 1399.
[36] O. Marty, and B. Pitaval (private communication).
[37] A. M. Mintairov and H. Temkin, Phys. Rev. B **55**, 5117 (1997).
[38] A. M. Mintairov, D. M. Mazurenko, M. A. Sinistin, and B. S. Yavich, Fiz. Tekh. Poloprovodn. **28**, 1550 (1994) [Semiconductors **28**, 866 (1994)].
[39] E. Burstein, in *Phonons and Phonon Interactions*, edited by T. A. Bak (Benjamin, New York, 1964).
[40] H. Rücker and M. Methfessel, Phys. Rev. B **52**, 11 059 (1995).
[41] M. Cardona, P. Etchegoin, H. D. Fuchs, and P. Molinàs-Mata, J. Phys.: Condens. Matter **5**, A61 (1993).
[42] H. D. Fuchs, P. Etchegoin, M. Cardona, K. Itoh, and E. E. Haller, Phys. Rev. Lett. **70**, 1715 (1993).
[43] J. M. Zhang, T. Ruf, M. Cardona, O. Ambacher, M. Stutzmann, J.-M. Wagner, and F. Bechstedt, Phys. Rev. B **56**, 14 399 (1997).
[44] J. M. Zhang, M. Giehler, A. Göbel, T. Ruf, M. Cardona, E. E. Haller, and K. Itoh, Phys. Rev. B **57**, 1348 (1998).
[45] M. Meléndez-Lira, J. Menéndez, W. Windl, O. F. Sankey, G. S. Spencer, S. Sego, R. B. Culbertson, A. E. Bair, and T. L. Alford, Phys. Rev. B **54**, 12 866 (1996).
[46] *Semiconductors: Group IV and III-V Compounds*, edited by O. Madelung, Landolt-Börnstein, New Series, Group X, Vol. 17, Pt. a (Springer-Verlag, Berlin, 1991).
[47] J. L. Martins and A. Zunger, Phys. Rev. B **30**, 6217 (1984).
[48] R. Carles, G. Landa, and J. B. Renucci, Solid State Commun. **53**, 179 (1985).
[49] In a bulk material under hydrostatic strain, $\Delta r/r$ is the relative change of the lattice constant and Eq. (4) reduces to the usual definition of the Grüneisen parameter (Refs. 50 and 51).
[50] E. Anastassakis, A. Pinczuk, E. Burstein, F. H. Pollak, and M. Cardona, Solid State Commun. **8**, 133 (1970).
[51] F. Cerdeira, C. J. Buchenauer, F. H. Pollak, and M. Cardona, Phys. Rev. B **5**, 580 (1972).
[52] A. Balzarotti, N. Motta, A. Kisiel, M. Zimnal-Starnawska, M. T. Czyzyk, and M. Podgórny, Phys. Rev. B **31**, 7526 (1985).
[53] P. Wickboldt, E. Anastassakis, R. Sauer, and M. Cardona, Phys. Rev. B **35**, 1362 (1987).
[54] K. Aoki, E. Anastassakis, and M. Cardona, Phys. Rev. B **30**, 681 (1984).
[55] S.-G. Shen and Y.-Q. Fan, Phys. Rev. B **50**, 1506 (1994).
[56] E. Anastassakis and M. Cardona, Phys. Status Solidi B **129**, 101 (1985).
[57] M. Holtz, M. Seon, O. Brafman, R. Manor, and D. Fekete, Phys. Rev. B **54**, 8714 (1996).
[58] R. Manor, O. Brafman, and R. F. Kopf, Phys. Rev. B **56**, 3567 (1997).
[59] D. T. Hon and W. L. Faust, Appl. Phys. **1**, 241 (1973).
[60] C^0_{GaAs} was taken from Ref. 61, and C^0_{InAs} deduced from measurements performed on an InAs(111) crystal.
[61] A. Anastassiadou, Y. S. Raptis, and E. Anastassakis, J. Appl. Phys. **60**, 2924 (1986).
[62] As collective oscillations of free carriers have often large damping constants, it is important to consider these interference effects when calculating the response of coupled LO-plasmon modes.
[63] A. M. Mintairov, K. E. Smekalin, V. M. Ustinov, and P. Khvostikov, Fiz. Tekh. Poloprovodn. **24**, 1539 (1990) [Sov. Phys. Semicond. **24**, 962 (1990)].